Dalton Transactions

Cite this: *Dalton Trans.*, 2012, **41**, 14257

www.rsc.org/dalton

PAPER

Water-soluble, redox-active organometallic calcium chelators†

Koyel X. Bhattacharyya, Leïla Boubekeur-Lecaque,‡* Issa Tapsoba, Emmanuel Maisonhaute,§ Bernd Schöllhorn¶ and Christian Amatore

Received 10th August 2012, Accepted 12th September 2012
DOI: 10.1039/c2dt31830j

This paper describes a new series of organometallic water-soluble chelators combining a redox moiety (ferrocene) and a selective Ca^{2+} chelator (BAPTA) separated by an ethynyl bridge. We report the synthesis and characterization of organometallic derivatives of the BAPTA chelator featuring one (**2a**) and two ferrocenyl (**2b**) moieties. Single crystal X-ray structural analysis on these chelators revealed unexpected conformations for the ferrocenyl substituent with respect to the phenyl ring of the BAPTA unit. DFT calculations on a model system of the ferrocenyl-ethynyl-BAPTA molecule were carried out to evaluate the energy separation between the two limiting conformations observed experimentally in the solid state, and to check the effective electronic communication between the binding pocket and the redox probe. The binding affinity of **2a–b** for Ca^{2+}, as probed by UV-Vis and cyclic voltammetry, revealed distinct behaviors in the presence of a metal ion depending on whether BAPTA is substituted by one or two ferrocenyl groups.

Introduction

Although metals represent just a small percentage of the total human body weight, they play a central role in many vital processes in biology such as respiration, enzymatic metabolism, nervous system activity, *etc.*[1,2] In the vast field of bioinorganic chemistry, our interest is focused on metals from the s-block which are known as information carriers and triggers for a wide range of biological processes, but that are difficult to monitor. In fact, these metals have no unpaired electrons, are diamagnetic and colourless, and therefore detection of rapid changes in concentration still represents a formidable challenge.

In particular, calcium as a chemical messenger is involved in a wide variety of cell functions and the local variation of its concentration plays a key role in the control of ion channels, muscle contraction or neurotransmitter secretion at nerve terminals.[3] The latter biochemical process is triggered by a sudden jump of calcium concentration in the intracellular medium that leads to vesicular fusion with the cellular membrane and ultimately to neurotransmitter secretion.[4] *In vitro* study of such a mechanism requires the precise control of Ca^{2+} concentration by means of Ca^{2+}-sequestrants that could be stimulated on-demand to release the free calcium. Among all possible physico-chemical stimuli, light has been the first one to be exploited to trigger calcium release and remains to date the most powerful approach.[5–8] It relies on the drastic decrease of Ca^{2+} affinity upon photolysis of the Ca^{2+}-sequestrant.[9–12] Alternatively, electrochemistry could be a more attractive approach to switch the affinity *via* oxidation or reduction of the sequestrant.[13–16] The switching could be reversible and might occur with high spatial and temporal resolution thanks to the intrinsic properties of ultramicroelectrodes.[17,18]

Our group has recently described a new organometallic derivative of the BAPTA ligand bearing a ferrocenyl, soluble in biocompatible media and highly selective for calcium over the most likely competing ions like magnesium.[14] However, the calcium affinity of this mono-ferrocenyl-BAPTA derivative proved to be barely affected by the oxidation of the ferrocenyl group even if fully conjugated with the chelating moiety. In that case, electrochemical studies in the presence of calcium showed an anodic shift for the oxidation of the ferrocenyl unit that could not be explained with the commonly accepted square scheme mechanism. For the purpose of improving the performance of redox-activated Ca^{2+} release, we envisaged the combination of two redox units with the chelating pocket. Here, we report the synthesis and characterizations of the bis-ferrocenyl-BAPTA derivative, which behaves differently than the mono-ferrocenyl-BAPTA previously described by our group. X-ray structures and DFT calculations also gave valuable information about the

Department of Chemistry, UMR 8640 CNRS-ENS-UPMC, Ecole Normale Supérieure, 24 rue Lhomond, 75005 Paris, France. E-mail: leila.boubekeur@univ-paris-diderot.fr

† Electronic supplementary information (ESI) available: CIF files, tables giving crystallographic data for compounds **2a–b**, molecular modeling coordinates, electrochemical data, and NMR spectra. CCDC 894007 and 894008. For ESI and crystallographic data in CIF or other electronic format see DOI: 10.1039/c2dt31830j

‡ Present address: Laboratoire Interfaces, Traitements, Organisation et Dynamique des Systèmes (ITODYS), CNRS UMR 7086, Université Paris Diderot, 15 rue Jean Antoine de Baïf, 75205 Paris Cedex 13, France.

§ Present address: Laboratoire Interfaces et Systèmes Electrochimiques – UPR 15, Université Pierre et Marie Curie-Paris 06, 75005 Paris, France.

¶ Present address: Laboratoire d'Electrochimie Moléculaire, Université Paris Diderot, UMR CNRS 7591, 15 rue Jean de Baïf, 75013 Paris, France.

electronic communication between the chelating moiety and the redox unit separated by an ethynyl bridge.

Results and discussion

Synthesis

The synthesis of the novel organometallic derivatives was carried out in six steps from 2-nitrophenol with the bromo-substituted BAPTA **1a–b** as key intermediates for the preparation of the desired ferrocene based ligands (see Scheme 1 and ESI†). The mono and bis-bromoBAPTA **1a**[19] and **1b**,[20] previously described in the literature, were used in the Sonogashira coupling reaction to form C–C bonds with ethynylferrocene. A Sonogashira coupling of derivative **1a** (and **1b**) with 1 equiv. (and 2 equiv., respectively) of ethynylferrocene provided the desired proligand **2a** (and **2b**, respectively) in 34 to 38% yield, which is satisfactory considering the highly deactivated nature of these bromoarenes incorporating two-electron donor substituents. Subsequent alkaline hydrolysis of the tetrakis esters **2a–b** yielded the corresponding tetrapotassium salts **3a–b**.

All compounds were characterized by NMR spectroscopy and microanalysis. Though the ^{1}H-NMR signals of the ferrocenyl moiety in **2a–b** resembled their ethynylferrocene precursor, the formation of the desired organometallic BAPTA ligands was clearly evidenced by the disappearance of the H–C≡C signal at 2.71 ppm and the high field shifting of aromatic signals in the BAPTA fragment. The ^{1}H NMR spectra of the tetraacetate ligands **3a–b** proved to be hardly exploitable as all signals are broadened. However, the disappearance of the triplet signal associated to the ethyl ester group is clear evidence of the complete deprotection of the tetrakis ester. Mass spectrometry and elemental analysis further confirmed the formation of **3a–b**.

X-ray crystal structures

Single-crystal X-ray structures were obtained for ligands **2a** and **2b** featuring one and two ferrocene moieties respectively. Representations of the molecular structures are shown in Fig. 1 and 2, and selected interatomic distances and angles are collected in Table 1.

Despite the importance of the BAPTA chelator, X-ray structures for BAPTA like compounds are very scarce in the literature. To the best of our knowledge, only three examples of BAPTA structures have been reported so far.[21–23] The single-crystal structures for the tetramethylester of the parent BAPTA and the fully protonated tetraacetic acid dianilinium BAPTA derivative are known. For the latter, the molecular structure is centrosymmetric with the central ethylene glycol moiety adopting an all-*trans* conformation (torsion angle O–C–C–O ~ 180°). Conversely, BAPTA-tetramethylester crystallizes as two crystallographically different molecules depending on the conformation of the ethylene glycol moiety. One type of molecule has the all-*trans* conformation, while the other type exhibits a torsion angle O–C–C–O of about 79°. The last remarkable structure is a calcium complex featuring a BAPTA with two F atoms in *para* positions to the N atoms (FBAPTA) coordinated to a Ca^{2+} ion. In that case, the central ethylene glycol moiety displays a torsion angle of 60.8°, allowing the Ca^{2+} ion to be coordinated by the eight donor atoms of the chelator. Therefore, it appears that the BAPTA motif has significant conformational flexibility ranging from the *gauche* to the all-*trans* conformations.

The central ethylene glycol moiety in ferrocenyl-BAPTA derivatives has a torsion angle α of 72.9 for ligand **2a** and 73.4° for ligand **2b**. These values indicate a molecular conformation between the expected all-*trans* conformation (α ~ 180°) for the free ligand and the *gauche* conformation observed for BAPTA

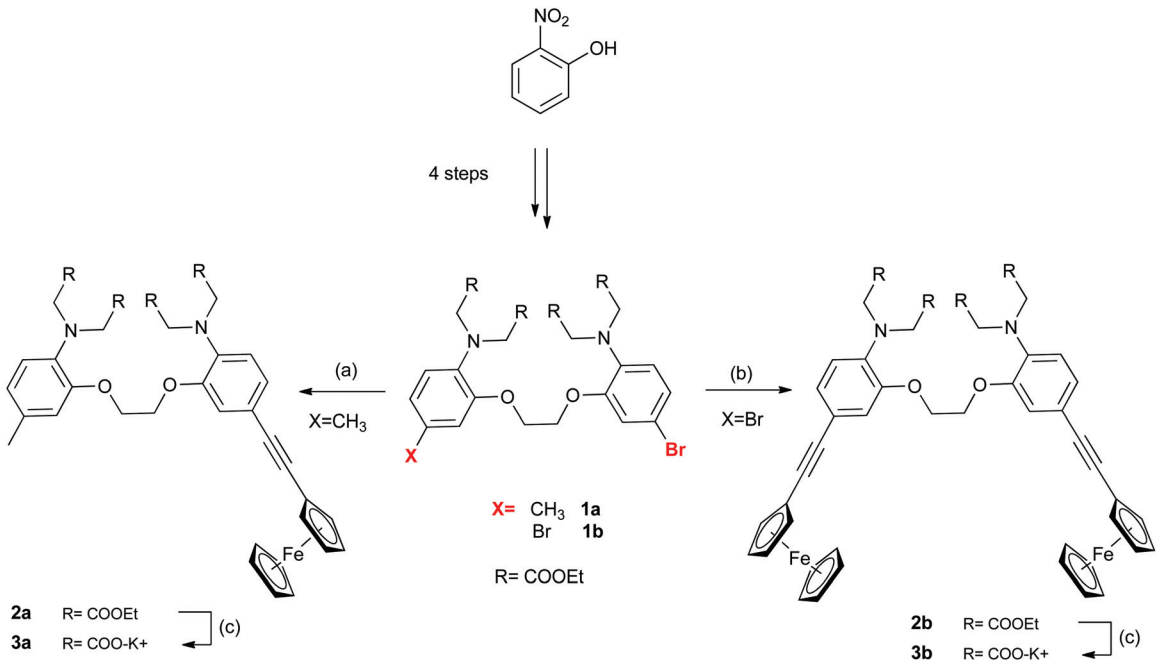

Scheme 1 Synthesis of ferroceneBAPTA chelators: (a) $PdCl_2(PPh_3)_2$, ethynylferrocene (1 equiv.), DMF, iPr_2NH, 110 °C (38%); (b) $PdCl_2(PPh_3)_2$, ethynylferrocene (2 equiv.), DMF, iPr_2NH, 110 °C (34%); (c) KOH, THF–water.

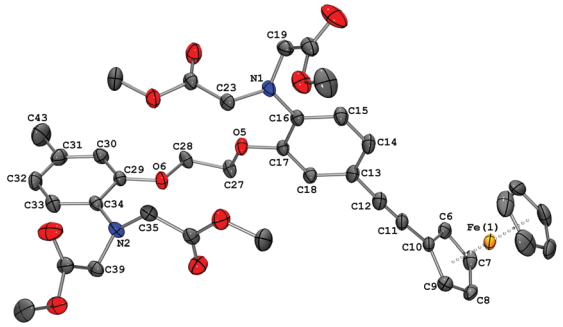

Fig. 1 Molecular structure of **2a** showing the atom numbering scheme with the ellipsoids drawn at the 50% probability level. For the sake of clarity, hydrogen atoms have been omitted and only one carbon of the ethyl ester groups is shown.

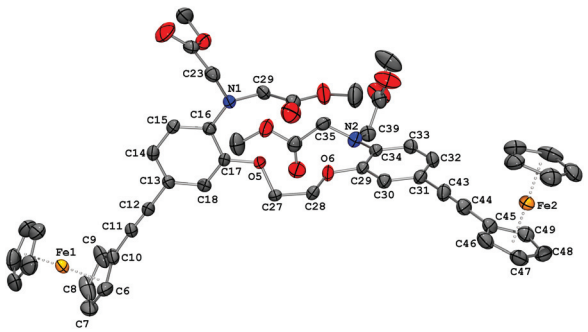

Fig. 2 Molecular structure of **2b** showing the atom numbering scheme with the ellipsoids drawn at the 50% probability level. For the sake of clarity, hydrogen atoms have been omitted and only one carbon of the ethyl ester groups is shown.

derivatives coordinated to Ca^{2+}. The C≡C bond distances in **2b** are 1.175(4) and 1.177(4) Å and slightly longer in **2a** (1.193(5) Å), which are in agreement with those in the parent (phenyl-ethynyl)ferrocene described in the literature.[24] The Cp rings of the ferrocene groups deviate slightly from the eclipsed conformation, as evidenced by the average C–C_g^s–C_g^u–C torsion angles of 5 and 6°, where C_g^s and C_g^u are the substituted and unsubstituted Cp ring centroids. The Cp rings in each molecule are almost parallel since the angles between the Cp rings planes range from 1.3 to 3.0°.

It is worth mentioning that the substituted Cp and phenyl rings adopt various conformations in the solid state. Indeed, the crystal structure of **2b** shows that the angles between the Cp and the phenyl rings are 21.4 and 79.2° in the same molecule, which correspond to the nearly coplanar and orthogonal conformations. Conversely, the monoferrocenyl-BAPTA **2a** exhibits only a nearly perpendicular orientation of the phenyl ring with respect to the Cp plane, with an angle of 87.8°. It is interesting to note that the arrangement of the Cp and phenyl rings is different from that predicted on the basis of DFT calculations. The latter performed on a model system of ferrocenyl-BAPTA **II** (see Fig. 3a) and reported previously by our group suggested that the coplanar conformation **A** is the most stable (*vide infra* DFT calculations).

Various X-ray structures for ferrocenylethynyl substituted aromatics reported in the literature show that the relative orientation

Table 1 Selected bond lengths (Å), angles (°) and torsion angles (°) for **2a** and **2b**

	2a	**2b**
C27–C28	1.500(4)	1.488(4)
N1–C16	1.395(4)	1.391(4)
N2–C34	1.410(4)	1.392(4)
C11–C12	1.193(5)	1.175(4)
C43–C44	—	1.177(4)
C12–C13	1.438(4)	1.452(4)
C10–C11	1.429(4)	1.414(4)
C31–C43	1.514(5)	1.434(5)
C44–C45	—	1.426(5)
C9–C10–C13–C14	90	83
C30–C31–C45–C46	—	−21
O5–C27–C28–O6	−73	−73
Sum of angles around N1	356.0	357.2
Sum of angles around N2	355.6	356.9

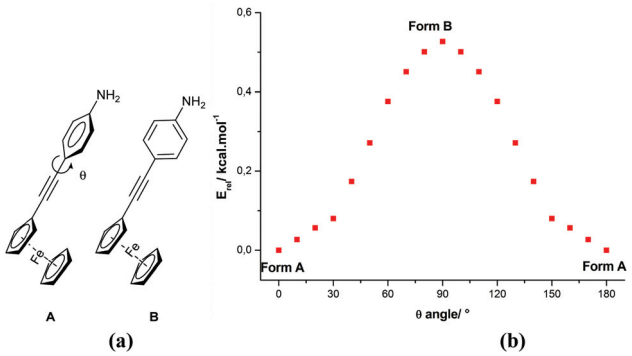

Fig. 3 (a) Model system **II** for the two limiting conformations: coplanar (form **A**) and perpendicular (form **B**); (b) evolution of the relative energy of conformations *versus* the twisting angle θ (functional B3PW91, basis set: 6-31+g* (C, H, N); Lanl2dz (Fe)).

of the Cp and the aromatic separated by an ethynyl bridge ranges from perpendicular to coplanar conformations that could be governed either by electronic effects and/or crystal packing.[25] (Pentafluorophenyl)ethynyl-ferrocene[26] and phenylethynylferrocene,[24] which adopt in the solid state the coplanar and the perpendicular conformations respectively, are a good illustration of the diversity found in such structures.

However, we must bear in mind that the relative orientation of the ferrocenyl redox moiety and the aromatic chelating entity is an important question in this series of redox-switchable chelators. In fact, the good electronic communication between these two parts of the ligand (π conjugation) is a crucial requirement for the remote redox switching. This apparent contradiction between theory and experience led us to investigate the effect of twisting the angle θ on the stability of the phenylethynylferrocene.

DFT calculations

DFT calculations on a model system for conformations **A** (coplanar, $\theta = 0°$) and **B** (perpendicular, $\theta = 90°$) have been carried out to evaluate the energy difference between these two limiting conformations observed experimentally (Fig. 3a). As mentioned

above, previously reported studies on a model system of ferrocenylBAPTA have shown that the energy minimized structure predicted from DFT calculations in the gas phase is the coplanar conformation **A**.

In order to estimate the rotational barrier between the two conformers, a series of calculations were performed on **II** in which the dihedral angle θ was varied from 0 to 90° in 10° increments. The energy calculations were performed on optimized constrained geometries in which the dihedral angle θ was the only frozen internal coordinate. The energy increases steadily with the angle θ and reaches a maximum for 90° corresponding to conformation B (Fig. 3b). Frequency calculations further confirmed the transition state nature of this stationary point (a single imaginary frequency). The normal mode associated with this imaginary frequency is the torsion of the phenyl ring around the C≡C linker that is expected as the reaction coordinate for such a conformational change. The negligible energy difference in the gas phase at room temperature between the coplanar and the perpendicular forms indicates nearly unhindered rotation around the C–C bond. Considering the adopted conformations in the crystal structures of **2a** and **2b**, the forms **A** and **B** are respectively absolute and local minima. Therefore, theoretical calculations suggest that the slight energy increase due to electronic effects could be easily counterbalanced by the crystal packing, favoring in some cases the perpendicular conformation **B**.

Population analysis on the two conformers **A** and **B** shows that the electronic delocalization is not disrupted in the perpendicular conformation but involves the second π system of the ethynyl spacer (Fig. 4). Therefore, the free rotation of the ferrocene unit around the C–C bond should barely affect the electronic communication between the redox moiety and the nitrogen lone pair.

Conversely, molecular modeling of the BAPTA–Ca^{2+} complex in the gas phase and the reported X-ray structure of this complex reveals structural distortions from planarity with rotation around the C(aryl)–N bond as required for the coordination of Ca^{2+}.[21,27] Along with the conformational change, the nitrogen lone pair is no longer involved in the π system of the phenyl ring, but instead takes part in calcium binding.[14]

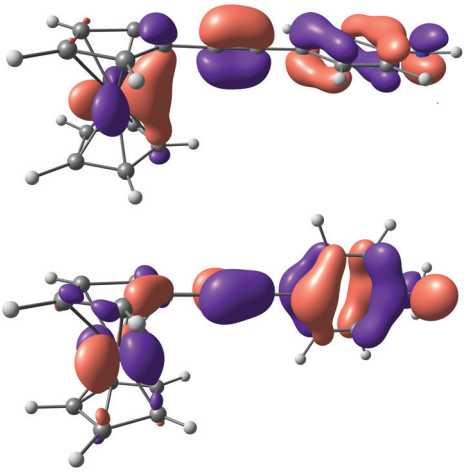

Fig. 4 HOMO orbital for model system **II** in: (up) coplanar conformation **A**; (bottom) perpendicular conformation **B**. Contour values are plotted at ±0.04 (e $bohr^{-3}$)$^{1/2}$ for molecular orbitals.

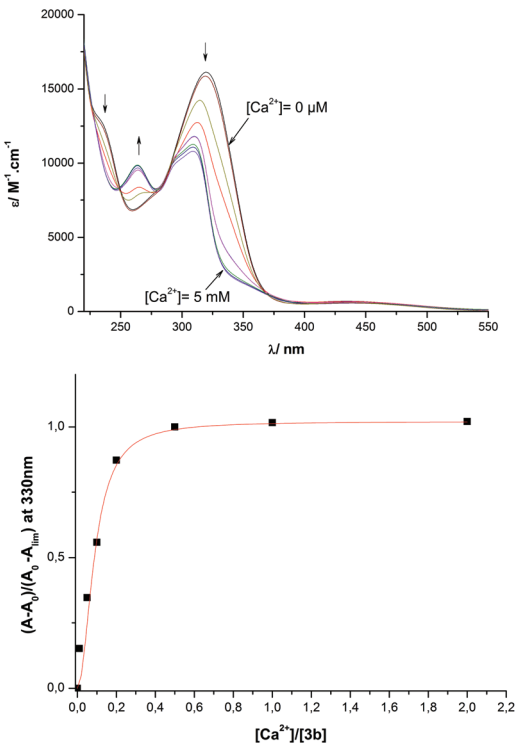

Fig. 5 (up) UV-Vis absorption spectra of **3b** for different Ca^{2+} concentrations ($[\mathbf{3b}]_0$ = 100 µM, 0.1 M KCl, 30 mM MOPS pH = 7.2). (bottom) Evolution of the normalized absorbance at 330 nm, where A and A_0 are the absorbance at 330 nm of the solution at a given ratio $[\mathbf{Ca^{2+}}]/[\mathbf{3b}]$ and of the free ligand **3b**, respectively. The red curve following the data points is only a guide to the eye.

UV-Vis studies

UV-Visible spectroscopy (UV-Vis) and cyclic voltammetry (CV) studies were conducted in buffered aqueous solutions to evaluate the calcium affinity of ligands **3a–b**. The chelator **3a** has been previously reported in a short communication.[14] In the absence of calcium, **3a** mainly exhibits two absorption maxima at 319 nm ($\varepsilon = 3 \times 10^4$ M^{-1} cm^{-1}) and 430 nm ($\varepsilon = 2 \times 10^3$ M^{-1} cm^{-1}). The large absorbance band in the 270–380 nm range shifts to shorter wavelengths upon calcium binding. Conversely, the weaker band around 430 nm is barely affected by the increase in the calcium concentration. In the presence of increasing amounts of Ca^{2+}, the absorbance at two wavelengths (266 and 326 nm) follows a standard saturation behavior that has been fitted with a 1L : 1Ca^{2+} model. A least squares minimization provided a dissociation constant K_d^{Ca} of 320 ± 8 nM (at 22 ± 2 °C, pH = 7.2) for ligand **3a** (see Fig. S8 in the ESI†).

In the absence of Ca^{2+}, the UV-Vis spectrum recorded for the bis-ferrocenyl **3b** is almost the same as the one described for **3a** and does not deserve further comment. In the presence of increasing amounts of Ca^{2+}, the titration curves for chelator **3b** show clean isosbestic points (at 226, 250, 285 and 370 nm; see Fig. 5), indicative of the co-existence of only two species in

solution (the free ligand and the complex). Although the absorbance at a given wavelength follows standard saturation behavior, the saturation is achieved at a ratio Ca^{2+}/L of 0.5 instead of 1. All attempts to fit the data points at a given wavelength with a 1 : 1 stoichiometry model (nonlinear least squares analysis of the absorbance *A versus* the pre-equilibrium concentration c_M of Ca^{2+}) failed. For other stoichiometries, it should be noted that there is no explicit expression of the absorbance *versus* the total Ca^{2+} concentration c_M if the approximation $[Ca^{2+}] \approx c_M$ is not valid.[28] Therefore, we were not able to treat the data quantitatively to extract the affinity constant of the bis-ferrocenyl derivative **3b** for Ca^{2+}.

Electrochemistry

Taking advantage of the redox probe incorporated into the chelator, the electrochemical behavior of the free ligands **3a–b** and the effect of sequential additions of Ca^{2+} were investigated by CV in buffered aqueous solutions at pH 7.4. The free ligand is characterized in both cases by two redox processes. The first reversible response at 250 mV (*vs.* SCE) involves the iron center of the ferrocene moiety.[29] The second irreversible process, whose anodic peak potential is at 750 mV (*vs.* SCE) for **3a**[14] and 605 (*vs.* SCE) for **3b**, stems from the irreversible oxidation of the aromatic amino groups (see Fig. S5 in the ESI† for the CV curve of the free ligand **3b**).

The electrochemical responses of chelators where complexation/decomplexation reactions are coupled to redox processes (square scheme mechanism) have been thoroughly studied by means of theoretical and experimental tools.[30–35] Two limiting electrochemical behaviors ("two-wave" *vs.* "anodic shift") are described in the literature in the presence of sub-stoichiometric amounts of cations. The electrochemical behaviors of these closely related ligands **3a** and **3b** in the presence of calcium proved to be very different. Indeed, as shown in our previous publication, gradual increase of Ca^{2+} concentration in an aqueous electrolyte containing ligand **3a** led to a progressive anodic shift of the ferrocene/ferrocenium redox couple and reached a limit of 80 mV for 1 equiv. of Ca^{2+}. A further increase of Ca^{2+} concentration had no significant effect on the above mentioned oxidation peak which is consistent with the 1 : 1 stoichiometry deduced from UV-Vis studies. Digital CV simulations of the square scheme mechanism reported elsewhere[14] and based on the set of parameters obtained experimentally for ligand **3a** have clearly shown that even for our rather small potential separation, two-wave behavior should be observed, such that two separate redox signals (free and complexed ligands) appear at potentials that are independent of calcium concentration. Therefore, a more involved mechanism coupling complexation to electron transfer governs the unexpected anodic shift behavior of ligand **3a**. The electrochemical behavior of the bis-ferrocenyl derivative **3b** is more subtle.

One can distinguish two regimes depending on the free calcium concentration (see Fig. 6). At very low Ca^{2+} concentrations, the voltammetric response exhibits the original oxidation wave corresponding to the free ligand and a new wave at 350 mV assigned to a calcium complex. As the concentration of Ca^{2+} increases in the medium, the current associated with the new wave increases at the expense of the original wave of the free ligand. In this first regime, the electrochemical behavior of **3b** corresponds to the so-called "two-wave behavior". In the backward scan, only one reduction wave is observed and seems unaffected by the increase in Ca^{2+} concentration in the medium. This reduction wave associated with the free ligand points to the dissociation of the oxidized form of the complex and a slow recomplexation equilibrium. In a second regime corresponding to higher Ca^{2+} concentrations, a shifting behavior toward a more anodic potential is observed, as in the case of ligand **3a** but accompanied by an increase in the current peak amplitude. Moreover, at a given Ca^{2+} concentration, the current peak follows a linear behavior with respect to scan rate, which points to a diffusionless process (see Fig. 6). This fact reveals the oxidation of adsorbed species on the electrode surface. The charge passed to oxidize the adsorbed complex (integration of the area under the *i–E* curves) allowed us to estimate a surface coverage of electroactive species of about 7.5×10^{-11} mol cm^{-2}. At a given ratio ligand/Ca^{2+}, this surface coverage increases dramatically with time as evidenced by the CV curves obtained immediately after introduction of a large excess of Ca^{2+} and 2 h after addition (see Fig. S6 in the ESI†).

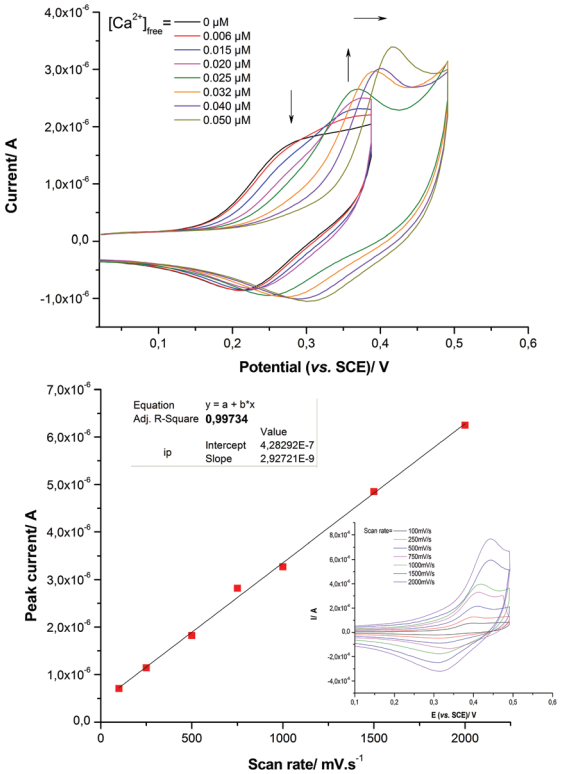

Fig. 6 Effect of Ca^{2+} concentration on the electrochemical response of **3b** (1 mM): (up) cyclic voltammetry at 0.5 V s^{-1}; (bottom) evolution of the oxidation peak current *versus* the scan rate, the free calcium concentration is set by the EGTA buffer at 50 nM.

The two-wave behavior evidenced for **3b** at very low free Ca^{2+} concentrations, that are only accessible in an ion-buffered medium, is evidenced when the free Ca^{2+} concentration is set by the EGTA ion buffer. In the absence of EGTA Ca^{2+}-buffer, the electrochemical behavior of **3b** follows an anodic shift.

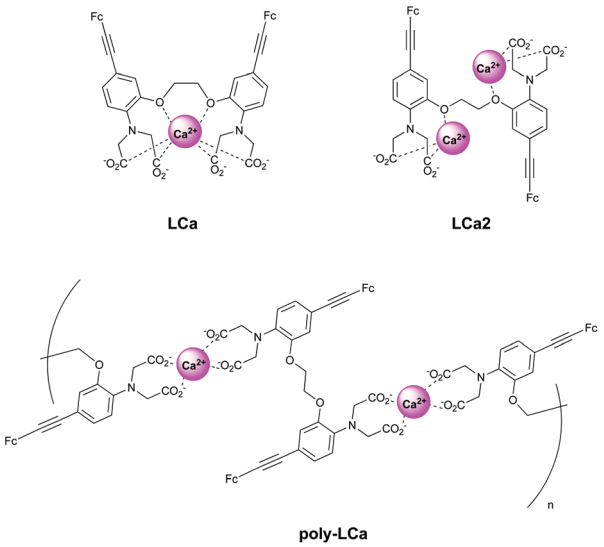

Scheme 2 Suggested Ca^{2+} complex structures involving ligand **3b**.

Conversely, the monoferrocenyl-BAPTA derivative **3a** undergoes an anodic shift in the presence of Ca^{2+} irrespective of the presence of EGTA buffer.

The intricate electrochemical behavior of **3b** in the presence of Ca^{2+} suggests the occurrence of different complex stoichiometries in the medium depending on the free Ca^{2+} concentration. Considering the flexibility of the ethylene glycol unit in the BAPTA structure and the number of donor atoms, it is not unreasonable to envisage complex structures such as the neutral complex LCa_2 or the polymeric complex poly-LCa, as depicted in Scheme 2.

Experimental section

General considerations

All reactions were performed under argon if not otherwise stated. EGTA (ethylene glycol bis(2-aminoethyl ether)-*N*,*N*,*N*′,*N*′-tetraacetic acid), MOPS (4-morpholinepropanesulfonic acid), and BAPTA (1,2-bis(*o*-aminophenoxy)ethane-*N*,*N*,-*N*′,*N*′-tetraacetic acid) and all other chemicals were purchased from Sigma/Aldrich (France) or Alfa Aesar (France). 5-Bromo-5′-methyl-BAPTA tetraester **1a** and (5,5′)-dibromo-BAPTA tetraester **1b** were synthesized in four steps according to published procedures.[19,20] ^{1}H and ^{13}C-NMR spectra were recorded on a Brüker AC-250 spectrometer in the solvents indicated at 298 K. Chemical shifts are reported using the deuterated (^{13}C NMR) or the residual monoprotonated (^{1}H NMR) solvent signals as a reference. Mass spectra were recorded using a Jeol JMS-700 spectrometer. Elemental analyses were conducted at the Service de Microanalyses-ICSN (Gif sur Yvette, France). Thin layer chromatography (TLC) was performed on aluminium sheets precoated with 60 F_{254} silica gel. Preparative flash chromatography was performed on silica gel 60 (0.040–0.063 mm, Merck).

Synthesis of bis(ethynylferrocene)BAPTA tetraester 2b. An Ar-flushed round-bottomed Schlenk flask was charged with CuI (27 mg, 0.141 mmol), $PdCl_2(PPh_3)_2$ (99 mg, 0.141 mmol), PPh_3 (148 mg, 0.563 mmol), and an Ar-purged mixture of 1 : 1 DMF: i-Pr_2NH (10 mL). The mixture was stirred under Ar at 0 °C for 15 min. Ethynylferrocene (290 mg, 1.38 mmol) and dibromo-BAPTA tetraester **1b** (500 mg, 0.67 mmol) were added under Ar flow. The reaction was warmed to RT slowly, whereupon it was heated to 120 °C and stirred at reflux for 24 h. It was cooled to RT and dried on the Rotavap. The crude mixture was purified on a silica gel column in petroleum ether with increasing volumes of ethyl acetate to yield **2b** (230 mg, 34%) as an orange crystalline solid. ^{1}H-NMR (250 MHz, $CDCl_3$): δ 7.02 (dd, 2H, $^3J_{HH}$ = 8.2 Hz and $^4J_{HH}$ = 1.7 Hz, Ph), 6.96 (d, 2H, $^4J_{HH}$ = 1.7 Hz, Ph), 6.71 (d, 2H, $^3J_{HH}$ = 8.2 Hz, Ph), 4.48 (pseudo t, 4H, $^3J_{HH}$ = 1.8 Hz, CH of Cp-≡), 4.29 (s, 4H, CH_2O_{ether}), 4.24 (s, 10H, CH unsubstituted Cp), 4.22 (pseudo t, 4H, $^3J_{HH}$ = 1.8 Hz, CH of Cp-≡), 4.16 (s, 8H, CH_2N), 4.07 (q, 8H, $^3J_{HH}$ = 7.1 Hz, CH_2O_{ester}), 1.17 (t, $^3J_{HH}$ = 7.1 Hz, 12H, CH_3); ^{13}C-NMR (62.5 MHz, $CDCl_3$): δ 171.3 (C═O), 149.6 (C^{Ar}–O_{ether}), 139.4 (C^{Ar}–N), 125.1 (C^{Ar}–H), 118.3 (C^{Ar}–H), 117.0 (C^{Ar}-≡), 115.8 (C^{Ar}–H), 87.0 and 85.8 (–C≡C–), 71.2 (CH of substituted Cp ring), 69.9 (CH of unsubstituted Cp ring), 68.7 (CH of substituted Cp ring), 67.1 (CH_2–O_{ether}), 65.6 (quaternary C, Cp), 60.9 (CH_3–***C***H_2), 53.5 (CH_2–N), 14.0 (***C***H_3–CH_2); elemental analysis: calc. for $C_{54}H_{56}Fe_2N_2O_{10}\cdot CH_3COOEt$: C 63.74, H 5.90, N 2.56, found: C 63.64, H 5.68, N 2.71.

Synthesis of bis(ethynylferrocene)BAPTA potassium salt 3b. A solution of KOH 1 M in H_2O (325 μL) was added to a solution of **2b** (50 mg, 0.050 mmol) dissolved in THF (5 mL). The resulting mixture was stirred at rt for 18 h. The light-colored liquid phase above was decanted, and the oily residue was dried to an orange solid **3b** (>98%). The solid was redissolved in MeOH, filtered, and dried again on the Rotavap (42 mg, 73%). ESI-MS (*m*/*z*): 929.2 ([M^{4-}, K^+, $2H^+$]: *z* = 1); 891.1 ([M^{4-}, $3H^+$]: *z* = 1), 464.6 ([M^{4-}, K^+, H^+]: *z* = 2), 445.5 ([M^{4-}, $2H^+$]: *z* = 2). Elemental analysis: calc. for $C_{46}H_{36}Fe_2K_4N_2O_{10}\cdot 2H_2O\cdot 2MeOH$: C 50.35, H 4.23, N 2.45, found: C 50.49, H 4.67, N 2.26.

Electrochemistry

The electrochemical experiments in aqueous electrolyte were conducted in an air-tight three-electrode glass cell under an argon atmosphere, run by a computer-controlled potentiostat (Autolab PGSTAT 30, Eco-Chemie, the Netherlands). A large platinum wire and a saturated calomel electrode were used as a counter electrode and a reference electrode, respectively. A glassy carbon electrode with a disk radius of 0.5 mm was used as a working electrode. The working electrode was polished to a mirror finish before each experiment. The supporting electrolyte employed was prepared from ultra-pure water (>18 MΩ cm) and contained 0.1 M KCl, EGTA 10 mM and 30 mM MOPS, pH = 7.4. Cyclic voltammograms (CV) were recorded at room temperature (22 ± 2 °C). Square wave voltammetric parameters were as follows: initial potential 0.0 V, end potential 0.5 V, pulse amplitude 10.0 mV, step potential 1.0 mV, and frequency 25 Hz.

UV-Visible spectroscopy

All spectra were recorded on a computer-controlled Lambda 45-Perkin Elmer spectrophotometer. All spectroscopic measurements

were performed in aqueous solutions containing 0.1 M KCl, 10 mM MOPS pH = 7.2 adjusted with KOH. The affinity constant of chelator **3a** (10 μM) for Ca^{2+} was obtained by titration in pH and buffered Ca^{2+} (with 10 mM EGTA as the calcium buffer) aqueous media and data processed in the Hill plot (see ESI† and published communication[14]). UV-Vis studies for **3b** were conducted by direct titration with sequential additions of a solution of $CaCl_2$ until full saturation is reached ([Ca^{2+}]/[**3b**] = 50 equiv.). Data were analysed at different wavelengths and the normalized absorbance ($(A - A_0)/(A_0 - A_{lim})$) *versus* the ratio [$Ca^{2+}$]/[**3b**] plotted. Since the free Ca^{2+} concentration could not be approximated by the total Ca^{2+} concentration c_M, the Benesi–Hildebrand model is not applicable. However, in the case of a 1 : 1 complex stoichiometry, an explicit expression of the absorbance *versus* the total Ca^{2+} concentration c_M can be derived without approximation from the second order equation:

$$c_L x^2 - (c_L + c_M + K_d)x + c_M = 0 \quad (1)$$

where $x = (A - A_0)/(A_0 - A_{lim})$, A_0 (A_{lim}) is the absorbance at $c_M = 0$ (at full saturation respectively), A the absorbance at a given c_M, $c_M = [Ca^{2+}]_{free}$ + [Ca-complex], $c_L = [L]_{free}$ + [Ca-complex] and K_d the dissociation constant. The explicit expression of the absorbance A *versus* c_M is a solution of the second order equation (eqn (1)). K_d can thus be obtained by a nonlinear least squares minimization.

X-ray structural determination

Suitable yellow plate-like crystals of **2a** and orange block-like crystals of **2b** were grown by diffusion of hexanes into dichloromethane solutions at room temperature. The data were collected on Bruker ApexII-CCD (for **2a**) and Bruker-Nonius Kappa-CCD (for **2b**) X-ray diffractometers by using graphite-monochromated MoKα radiation (wavelength = 0.71073 Å). Unit-cell parameter determinations, data collection strategies, and integrations were carried out with the Bruker APEX2/SAINT[36] and Nonius EVAL-14 suite of programs[37] for **2a** and **2b** respectively. The data were corrected from absorption by a multi-scan method.[38] The structures were solved by direct methods and refined by full-matrix least-squares on all F_0^2 data using SHELXS-97[39] and SHELXL-97.[40,41] All non-hydrogen atoms were refined anisotropically, and H atoms bonded to C atoms were placed at calculated positions. Crystallographic data and refinement details are presented in Table 2. Structural analyses and drawings were made using ORTEP-3[42] and POV-ray 3.6 software. Crystallographic data for the structure reported in this paper have been deposited with the Cambridge Crystallographic Data Centre as supplementary publication no. CCDC-894007 and 894008.

DFT calculations

All calculations were carried out using the Gaussian 03-E.01 suite of programs.[43] The hybrid B3PW91 functional[44,45] was used for the DFT calculations and the basis set consisted of the 6-31+G* basis functions for H, C and N.[46,47] The LANL2DZ basis set consisting of *Effective Core Potential* (ECP) and double-ζ quality functions for valence electrons was employed for Fe.[48] All stationary points were characterized through the number of negative eigen values in their Hessian matrices. No symmetry constraints were imposed during structural optimizations. The energy calculations were performed on optimized constrained geometries in which the dihedral angle θ was the only frozen internal coordinate.

Table 2 Crystallographic data and refinement details for **2a** and **2b**

	2a	**2b**
Formula	$C_{44}H_{52}Cl_2FeN_2O_{10}$	$C_{54}H_{56}Fe_2N_2O_{10}$
F_w	895.63	1004.71
Crystal system	Triclinic	Triclinic
Space group	$P\bar{1}$	$P\bar{1}$
a/Å	12.9797(10)	12.9200(15)
b/Å	13.0797(10)	13.1070(14)
c/Å	13.7456(11)	18.3190(15)
α/°	96.115(5)	69.343(8)
β/°	101.424(4)	77.511(7)
γ/°	93.178(4)	62.753(7)
V/Å^3	2267.3(3)	2575.1(5)
Z	2	2
T/K	200(2)	250(2)
λ/Å	0.71073	0.71073
D_{calc}/g cm^{-3}	1.312	1.296
μ/mm^{-1}	0.507	0.621
Reflns collected	15 326	14 955
Ind. reflns (R_{int})	9669 (0.0673)	6751 (0.0446)
GOF on F^2	1.147	1.018
Final R, wR_2 [$I > 2\sigma(I)$]	0.0456, 0.0995	0.0501, 0.0851
All data	0.0844, 0.1246	0.1139, 0.1084

Conclusions

The two electrochemically active, water-soluble organometallic complexes whose synthesis and characterization have been described in this paper, **2a** and **2b**, represent a new family of BAPTA derivatives featuring a redox probe while maintaining excellent affinity and selectivity for Ca^{2+}. The structural characterization highlighted the diversity of conformations adopted by such ferrocenyl-ethynyl-BAPTA and DFT calculations enabled us to quantify the energetic cost required to rotate the ferrocenyl group from a coplanar to a perpendicular conformation. The rich electrochemistry evidenced for **3b** in the presence of Ca^{2+} cannot be described by the commonly accepted square scheme mechanism and encourages us to explore other mechanisms coupling electron transfer to complexation. Work is currently underway to investigate the ability of the bis-ferrocenyl-BAPTA derivative **3b** to release calcium under potential stimulation.

Acknowledgements

This work was supported by the CNRS (UMR 8640 and LIA XiamENS), ENS, the Université Pierre et Marie Curie, the ANR through REEL Blan06-2_136291 and the Franco-American Commission through the Fulbright advanced student fellowship (KXB).

References

1 I. Bertini, H. B. Gray, S. J. Lippard and J. S. Valentine, *Bioinorganic Chemistry*, University Science Books, Mill Valley, Calif., 1994.

2 K. L. Haas and K. J. Franz, *Chem. Rev.*, 2009, **109**, 4921–4960.
3 G. C. R. Ellis-Davies, *Chem. Rev.*, 2008, **108**, 1603–1613.
4 C. Amatore, S. Arbault, M. Guille and F. Lemaitre, *Chem. Rev.*, 2008, **108**, 2585–2621.
5 J. P. Y. Kao and R. Y. Tsien, *Biophys. J.*, 1988, **53**, 635–639.
6 S. R. Adams, J. P. Y. Kao, G. Grynkiewicz, A. Minta and R. Y. Tsien, *J. Am. Chem. Soc.*, 1988, **110**, 3212–3220.
7 S. R. Adams, J. P. Y. Kao and R. Y. Tsien, *J. Am. Chem. Soc.*, 1989, **111**, 7957–7968.
8 R. Y. Tsien, *Fluorescent Chemosensors for Ion and Molecule Recognition*, ACS Symposium Series, American Chemical Society, Washington, DC, 1993, vol. 538, pp. 130–146.
9 E. B. Brown, G. C. R. Ellis-Davis and W. W. Webb, *Biophys. J.*, 1998, **74**, A378–A378.
10 F. DelPrincipe, M. Egger, G. C. R. Ellis-Davies and E. Niggli, *Cell Calcium*, 1999, **25**, 85–91.
11 G. C. R. Ellis-Davies, *Biophotonics, Pt A*, 2003, **360**, 226–238.
12 H. Kasai, Y. Kanemoto, M. Matsuzaki, G. Ellis-Davis, A. Momotake, T. Arai, K. Hahn, Y. Wu, M. Ishikawa, J. Noguchi, T. Hayama, S. Watanabe and S. Morita, *Neurosci. Res.*, 2009, **65**, S3–S3.
13 C. Amatore, D. Genovese, E. Maisonhaute, N. Raouafi and B. Schöllhorn, *Angew. Chem., Int. Ed.*, 2008, **47**, 5211–5214.
14 K. X. Bhattacharyya, L. Boubekeur-Lecaque, I. Tapsoba, E. Maisonhaute, B. Schollhorn and C. Amatore, *Chem. Commun.*, 2011, **47**, 5199–5201.
15 R. Sahli, N. Raouafi, K. Boujlel, E. Maisonhaute, B. Schollhorn and C. Amatore, *New J. Chem.*, 2011, **35**, 709–715.
16 R. Sahli, N. Raouafi, E. Maisonhaute, K. Boujlel and B. Schollhorn, *Electrochim. Acta*, 2012, **63**, 228–231.
17 C. Amatore, in *Microelectrodes: Theory and Applications*, ed. I. Montenegro, A. Queiros and J. L. Daschbach, Kluwer Academic Publishers, Dordrecht, 1991, vol. 197, p. 269.
18 J. Heinze, *Angew. Chem., Int. Ed. Engl.*, 1993, **32**, 1268–1288.
19 G. Grynkiewicz, M. Poenie and R. Y. Tsien, *J. Biol. Chem.*, 1985, **260**, 3440–3450.
20 R. Y. Tsien, *Biochemistry*, 1980, **19**, 2396–2404.
21 J. T. Gerig, P. Singh, L. A. Levy and R. E. London, *J. Inorg. Biochem.*, 1987, **31**, 113–121.
22 M. Rademeyer, D. A. Barkhuizen and G. E. M. Maguire, *Acta Crystallogr., Sect. E: Struct. Rep. Online*, 2004, **60**, O213–O215.
23 J. W. Raynor, M. Chruszcz and W. Minor, *Acta Crystallogr., Sect. E: Struct. Rep. Online*, 2007, **63**, O754–O756.
24 M. Zora, C. Acikgoz, T. A. Tumay, M. Odabasoglu and O. Buyukgungor, *Acta Crystallogr., Sect. C: Cryst. Struct. Commun.*, 2006, **62**, M327–M330.
25 L. Cuffe, R. D. A. Hudson, J. F. Gallagher, S. Jennings, C. J. McAdam, R. B. T. Connelly, A. R. Manning, B. H. Robinson and J. Simpson, *Organometallics*, 2005, **24**, 2051–2060.
26 C. Zhang, H. L. Zhang, D. D. Dai and J. H. Liang, *Acta Crystallogr. Sect. E: Struct. Rep. Online*, 2010, **66**, M914–U507.
27 C. K. Schauer and O. P. Anderson, *J. Am. Chem. Soc.*, 1987, **109**, 3646–3656.
28 B. Valeur, in *Molecular Fluorescence: Principles and Applications*, Wiley-VCH, Weinheim, 1st edn, 2002, pp. 337–348.
29 C. Amatore, E. Maisonhaute, B. Schollhorn and J. Wadhawan, *ChemPhysChem*, 2007, **8**, 1321–1329.
30 P. D. Beer, P. A. Gale and G. Z. Chen, *Coord. Chem. Rev.*, 1999, **186**, 3–36.
31 P. D. Beer, P. A. Gale and G. Z. Chen, *J. Chem. Soc., Dalton Trans.*, 1999, 1897–1909.
32 A. E. Kaifer, *Acc. Chem. Res.*, 1999, **32**, 62–71.
33 A. E. kaifer and S. Mendoza, in *Comprehensive Supramolecular Chemistry*, ed. G. W. Gokel, Elsevier, New York, 1996, vol. 1, pp. 701–731.
34 S. Mendoza, E. Castano, Y. Meas, L. A. Godinez and A. E. Kaifer, *Electroanal.*, 2004, **16**, 1469–1477.
35 S. R. Miller, D. A. Gustowski, Z. H. Chen, G. W. Gokel, L. Echegoyen and A. E. Kaifer, *Anal. Chem.*, 1988, **60**, 2021–2024.
36 *Bruker APEX2 and SAINT*, Bruker AXS Inc., Madison, Wisconsin, USA, 2009.
37 A. J. M. Duisenberg, L. M. J. Kroon-Batenburg and A. M. M. Schreurs, *J. Appl. Crystallogr.*, 2003, **36**, 220–229.
38 R. H. Blessing, *Acta Crystallogr., Sect. A: Fundam. Crystallogr.*, 1995, **51**, 33–38.
39 G. M. Sheldrick, *SHELXS-97. Program for Crystal Structure Resolution*, Univ. of Göttingen, Göttingen, Germany, 1997.
40 G. M. Sheldrick, *SHELXL-97. Program for Crystal Structure Analysis*, Univ. of Göttingen, Göttingen, Germany, 1997.
41 G. M. Sheldrick, *Acta Crystallogr., Sect. A: Fundam. Crystallogr.*, 2008, **64**, 112–122.
42 L. J. Farrugia, *J. Appl. Crystallogr.*, 1997, **30**, 565.
43 M. J. Frisch, G. W. Trucks, H. B. Schlegel, G. E. Scuseria, M. A. Robb, J. R. Cheeseman, J. A. Montgomery, Jr., T. Vreven, K. N. Kudin, J. C. Burant, J. M. Millam, S. S. Iyengar, J. Tomasi, V. Barone, B. Mennucci, M. Cossi, G. Scalmani, N. Rega, G. A. Petersson, H. Nakatsuji, M. Hada, M. Ehara, K. Toyota, R. Fukuda, J. Hasegawa, M. Ishida, T. Nakajima, Y. Honda, O. Kitao, H. Nakai, M. Klene, X. Li, J. E. Knox, H. P. Hratchian, J. B. Cross, V. Bakken, C. Adamo, J. Jaramillo, R. Gomperts, R. E. Stratmann, O. Yazyev, A. J. Austin, R. Cammi, C. Pomelli, J. W. Ochterski, P. Y. Ayala, K. Morokuma, G. A. Voth, P. Salvador, J. J. Dannenberg, V. G. Zakrzewski, S. Dapprich, A. D. Daniels, M. C. Strain, O. Farkas, D. K. Malick, A. D. Rabuck, K. Raghavachari, J. B. Foresman, J. V. Ortiz, Q. Cui, A. G. Baboul, S. Clifford, J. Cioslowski, B. B. Stefanov, G. Liu, A. Liashenko, P. Piskorz, I. Komaromi, R. L. Martin, D. J. Fox, T. Keith, M. A. Al-Laham, C. Y. Peng, A. Nanayakkara, M. Challacombe, P. M. W. Gill, B. Johnson, W. Chen, M. W. Wong, C. Gonzalez and J. A. Pople, *A. GAUSSIAN 03 (Revision E.01)*, Gaussian, Inc., Wallingford CT, ed., 2004.
44 A. D. Becke, *J. Chem. Phys.*, 1993, **98**, 5648–5652.
45 J. P. Perdew and Y. Wang, *Phys. Rev. B*, 1992, **45**, 13244–13249.
46 T. Clark, J. Chandrasekhar, G. W. Spitznagel and P. V. Schleyer, *J. Comput. Chem.*, 1983, **4**, 294–301.
47 M. M. Francl, W. J. Pietro, W. J. Hehre, J. S. Binkley, M. S. Gordon, D. J. Defrees and J. A. Pople, *J. Chem. Phys.*, 1982, **77**, 3654–3665.
48 P. J. Hay and W. R. Wadt, *J. Chem. Phys.*, 1985, **82**, 270–283.

